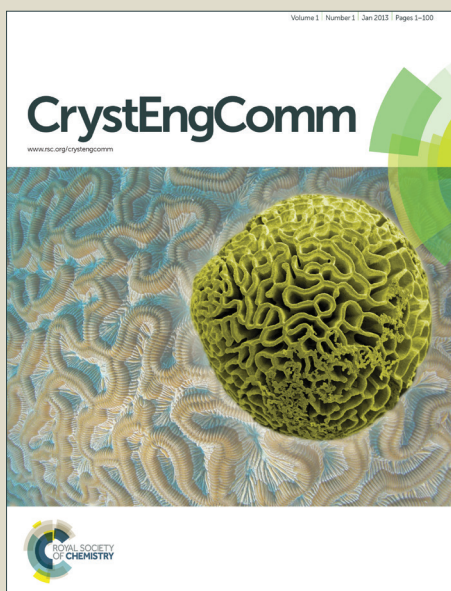


# CrystEngComm

Accepted Manuscript



This is an *Accepted Manuscript*, which has been through the Royal Society of Chemistry peer review process and has been accepted for publication.

*Accepted Manuscripts* are published online shortly after acceptance, before technical editing, formatting and proof reading. Using this free service, authors can make their results available to the community, in citable form, before we publish the edited article. We will replace this *Accepted Manuscript* with the edited and formatted *Advance Article* as soon as it is available.

You can find more information about *Accepted Manuscripts* in the [Information for Authors](#).

Please note that technical editing may introduce minor changes to the text and/or graphics, which may alter content. The journal's standard [Terms & Conditions](#) and the [Ethical guidelines](#) still apply. In no event shall the Royal Society of Chemistry be held responsible for any errors or omissions in this *Accepted Manuscript* or any consequences arising from the use of any information it contains.

## ARTICLE

# One-pot Solvothermal Synthesis of Well-ordered Layered Sodium Aluminoalcoholate Complex: A Useful Precursor for the Preparation of Porous Al<sub>2</sub>O<sub>3</sub> Particles†

Cite this: DOI: 10.1039/x0xx00000x

Received 00th xxxx 2013,  
Accepted 00th xxxx 2013

DOI: 10.1039/x0xx00000x

www.rsc.org/

Xiansen Li,<sup>\*1</sup> Vladimir K. Michaelis,<sup>2,3</sup> Ta-Chung Ong,<sup>2,3</sup> Stacey J. Smith,<sup>2</sup> Ian McKay,<sup>1</sup> Peter Müller,<sup>2</sup> Robert G. Griffin<sup>2,3</sup> and Evelyn N. Wang<sup>\*1</sup>

One-pot solvothermal synthesis of a robust tetranuclear sodium hexakis(glycolato)tris(methanolato)aluminate complex Na<sub>3</sub>[Al<sub>4</sub>(OCH<sub>3</sub>)<sub>3</sub>(OCH<sub>2</sub>CH<sub>2</sub>O)<sub>6</sub>] via a modified yet rigorous base-catalyzed transesterification mechanism is presented here. Single crystal X-ray diffraction (SCXRD) studies indicate that this unique Al complex contains three penta-coordinate Al<sup>3+</sup> ions, each bound to two bidentate ethylene glycolate chelators and one monodentate methanolate ligand. The remaining fourth Al<sup>3+</sup> ion is octahedrally coordinated to one oxygen atom from each of the six surrounding glycolate chelators, effectively stitching the three penta-coordinate Al moieties together into a novel tetranuclear Al complex. This aluminate complex is periodically self-assembled into well-ordered layers normal to the [110] axis with the intra-/inter-layer bindings involving extensive ionic bonds from the three charge-counterbalancing Na<sup>+</sup> cations rather than the more typical hydrogen bonding interactions as a result of the fewer free hydroxyl groups present in its structure. It can also serve as a valuable precursor toward the facile synthesis of high-surface-area alumina powders using a very efficient rapid pyrolysis technique.

## Introduction

Layered materials containing coordinatively unsaturated binding sites such as 5-coordinate Al (<sup>51</sup>Al) species are of topical interest because they promise improved performance for lithium-/sodium-ion batteries,<sup>1</sup> adsorbent,<sup>2</sup> and catalyst<sup>3</sup> applications. Among these, intercalated layered materials have attracted considerable attention due to their tunable pore size and versatile guest species such as Li<sup>+</sup> and Na<sup>+</sup> cations for increased adsorption capacity and selectivity. They are also important precursors towards preparing nanoscale porous lamellas,<sup>4</sup> nanotubes,<sup>5</sup> and composite materials.<sup>6</sup>

Solvothermal synthesis exhibits a significant advantage over conventional hydrothermal technique in cases where either moisture sensitive reagents or potential occurrence of insoluble metal hydroxide side-reactions is inevitably involved in the preparation. Solvothermal synthesis involving polyols (*e.g.*, 1,2-diols) as the solvent has so far been moderately explored for the preparations of novel zeolites,<sup>7</sup> silicopolyolate containing interesting <sup>51</sup>Si species,<sup>8</sup> and aluminoglycolate analogue containing fascinating <sup>51</sup>Al geometry.<sup>9</sup> For example, Gainsford *et al.* reported a trinuclear [Al<sub>3</sub>(OCH<sub>2</sub>CH<sub>2</sub>O)<sub>5</sub>(OCH<sub>2</sub>CH<sub>2</sub>OH)<sub>2</sub>]<sup>3-</sup> anion and several concomitant by-products prepared *via* direct reaction between alumina and NaOH in considerably excessive ethylene glycol (EG) solvent by slowly distilling off both EG and any liberated

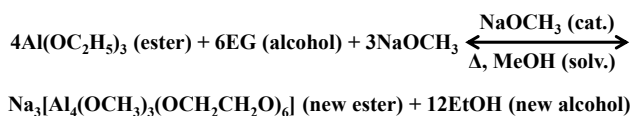
water from the reaction during the synthesis period until the pseudo-saturation state, followed by a recrystallization step.<sup>9d</sup>

Although the <sup>41</sup>Al and <sup>61</sup>Al species in zeolites, clays and minerals, *etc.* have been well studied,<sup>10</sup> relatively few <sup>51</sup>Al species have been reported in alkoxide-based crystalline solids to date.<sup>9,11</sup> Consequently, much less is known about their physicochemical properties, *e.g.*, the chemical-shift “fingerprint” region of <sup>27</sup>Al magic angle spinning nuclear magnetic resonance (MAS NMR) spectra for these unique <sup>51</sup>Al environments. The study of this unique structure is expected to extend the horizons of such existing systems. We herein report the asymmetric tetranuclear Al complex with three <sup>51</sup>Al species, which was achieved by using a modified transesterification synthetic strategy. In addition, we demonstrated the possibilities and benefits of using this layered Al complex as a valuable precursor for efficient preparation of high value-added nanoporous Al<sub>2</sub>O<sub>3</sub> powders that are of great relevance both academically and industrially as catalysts, catalyst supports, adsorbents, refractory ceramics, and active feedstocks.

## Results and Discussion

We present a novel solvothermal preparative method *via* a modified base-catalyzed transesterification mechanism, which is quite

scarcely explored for hybrid inorganic/organic materials preparations,<sup>12</sup> for the synthesis of a layered aluminoglycolate complex in the presence of methanol as a solvent rather than the more commonly used EG solvent. In the course of the solvothermal reaction, the effective deprotonation from the slightly excessive EG reactant is initially implemented by the action of an aliquot of strong base catalyst of sodium methoxide to initiate the S<sub>N</sub>2 nucleophilic substitution reaction, leading to the formation of bidentate ethylene glycolate chelators. These incoming chelators thus formed then compete with three aliquots of sodium methanolate for nucleophilic attack of the Al electrophiles, causing the concurrent departure of CH<sub>3</sub>CH<sub>2</sub>O<sup>-</sup> anions (Scheme 1). Due to the chelate nature of the bidentate glycolate ligand, Al electrophiles as ligand acceptors possess a coordinative preference for glycolate ligands over monodentate methanolate ones, thus affording a unique mixed <sup>[5]</sup>Al/<sup>[6]</sup>Al complex at a methanolate/glycolate ratio of 1:2 in the final empirical formula. The complexing power with central Al<sup>3+</sup> cations decreases in the following order: [OCH<sub>2</sub>CH<sub>2</sub>O]<sup>2-</sup> > CH<sub>3</sub>O<sup>-</sup> > CH<sub>3</sub>CH<sub>2</sub>O<sup>-</sup>. The NaOCH<sub>3</sub> catalyst is ultimately regenerated by reacting the resultant NaOCH<sub>2</sub>CH<sub>3</sub> with the MeOH formed in the first deprotonation step. It is worth noting that sodium methoxide in slight excess was employed as both the transesterifying base catalyst and one of the reactants. The newly formulated approach is unusual in that only single-step synthesis is utilized without any laborious cycles of fractional/vacuum-distillations required by previous researchers such as Gainsford *et al.*<sup>9d</sup> More importantly, this approach is versatile since it only implicates alkali metal alkoxide base-catalyzed alcoholysis but without any intervention of detectable alkaline (OH<sup>-</sup>) hydrolysis side-reactions.



**Scheme 1** Proposed reaction pathway to the target product Na<sub>3</sub>[Al<sub>4</sub>(OCH<sub>3</sub>)<sub>3</sub>(OCH<sub>2</sub>CH<sub>2</sub>O)<sub>6</sub>] starting with aluminium alkoxide, EG and sodium methoxide by a modified transesterification mechanism.

In the solvothermal synthesis, the conventional organic transesterification reaction was adapted such that the routine carboxylic acid ester was replaced with pseudo-covalent metal/non-metal alkoxide ester, as exemplified specifically in Scheme 1. This reversible S<sub>N</sub>2 nucleophilic substitution reaction involving a competitive ligand-exchange step is expected to be an efficient way to rationally tailor the relative contributions between the nucleation and crystal growth events, thus favoring the efficient large single crystal production. The alcohol-selective rule manifests the possibility of crystal composition tailoring by judiciously choosing different monohydroxy alcohols and polyols. Solvothermal crystallization at 181 °C for 5 days resulted in the end product with an actual chemical formula of Na<sub>3</sub>[Al<sub>4</sub>(OCH<sub>3</sub>)<sub>3</sub>(OCH<sub>2</sub>CH<sub>2</sub>O)<sub>6</sub>]. It is anticipated that the coupled high synthetic temperature and high autogenous vapor pressure<sup>13</sup> applied in the synthesis enable the formation of the largest tetranuclear Al complex of its kind ever reported in the literature. The multi-nuclear nature of this Al complex may explain its insolubility in MeOH, only slight solubility in water and EG, and enhanced stability against both hydrolysis and alcoholysis. This synthetic strategy is universal as long as the large electronegative metal/non-metal (*e.g.*, Si and B) can be prepared in the form of corresponding alkoxides, and is restricted neither by the insolubility of metal oxide/hydroxide in alkaline solutions nor by the potential formation of insoluble metal hydroxide impurities *in-situ* during synthesis, as encountered by other researchers.<sup>14</sup> Moreover,

the reactants are not only limited to alkoxide esters, but also include a variety of organic-soluble salts (*e.g.*, chlorides), organometallics and labile metal complexes over the corresponding metaloglycolate ones, although the latter category of reactions cannot be strictly classified as a transesterification reaction.

The details of the crystal structure and its structural refinement are listed in Table 1. The Al compound crystallizes in the monoclinic crystal system and space group P2<sub>1</sub>/c.

**Table 1** Crystallographic data and structural refinement for the Al complex.

Parameter	Data
CCDC No.	955650
Empirical formula	C <sub>15</sub> H <sub>33</sub> Al <sub>4</sub> Na <sub>3</sub> O <sub>15</sub> ·0.1CH <sub>4</sub> O
F.W.	633.35
Temp.	100(2) K
Wavelength	0.71073 Å
Crystal system	monoclinic
Space group	P2 <sub>1</sub> /c <i>a</i> = 11.2481(12) Å; <i>α</i> = 90°
Unit cell dimensions	<i>b</i> = 13.1877(14) Å; <i>β</i> = 105.738(2)° <i>c</i> = 18.235(2) Å; <i>γ</i> = 90°
Volume	2603.5(5) Å <sup>3</sup>
Z	4
Density (calculated)	1.616 mg/m <sup>3</sup>
Absorption coefficient	0.299 mm <sup>-1</sup>
<i>F</i> (000)	1319
Crystal size	0.11 × 0.04 × 0.01 mm <sup>3</sup>
<i>θ</i> collection range	1.88 to 30.99°
Index ranges	-16 ≤ <i>h</i> ≤ 15, -19 ≤ <i>k</i> ≤ 18, -26 ≤ <i>l</i> ≤ 26
Reflections collected	67765
Independent reflections	8270 [ <i>R</i> <sub>int</sub> = 0.0539]
Completeness to <i>θ</i> = 30.99°	99.7%
Absorption correction	Semi-empirical from equivalents
Max. and min. transmission	0.9970 and 0.9678
Refinement method	Full-matrix least-squares on <i>F</i> <sup>2</sup>
Data/restraints/parameters	8270/459/395
Goodness-of-fit on <i>F</i> <sup>2</sup>	1.046
Final <i>R</i> indices [ <i>I</i> > 2σ( <i>I</i> )]	<i>R</i> 1 = 0.0405, <i>wR</i> 2 = 0.0994
<i>R</i> indices (all data)	<i>R</i> 1 = 0.0633, <i>wR</i> 2 = 0.1110
Largest diff. peak and hole	0.521 and -0.438 e.Å <sup>-3</sup>

As determined by SCXRD, the asymmetric unit (AU) in the crystal structure contains one sodium hexakis(glycolato)tris(methanolato)aluminum complex Na<sub>3</sub>[Al<sub>4</sub>(OCH<sub>3</sub>)<sub>3</sub>(OCH<sub>2</sub>CH<sub>2</sub>O)<sub>6</sub>] (Fig. 1). Three of the four Al<sup>3+</sup> ions reside in considerably distorted <sup>[5]</sup>Al environments of rectangular pyramidal geometries rather than the more expected trigonal bipyramids by inspecting the O-Al-O bond angles. The remaining fourth Al<sup>3+</sup> ion in the complex is octahedrally coordinated to one oxygen atom from each of the six glycolate units in the AU, effectively tethering together the three surrounding <sup>[5]</sup>Al monomers into a tetranuclear configuration (*i.e.*, secondary building unit (BU)) by sharing the basal edges of AlO<sub>5</sub> pentahedra.

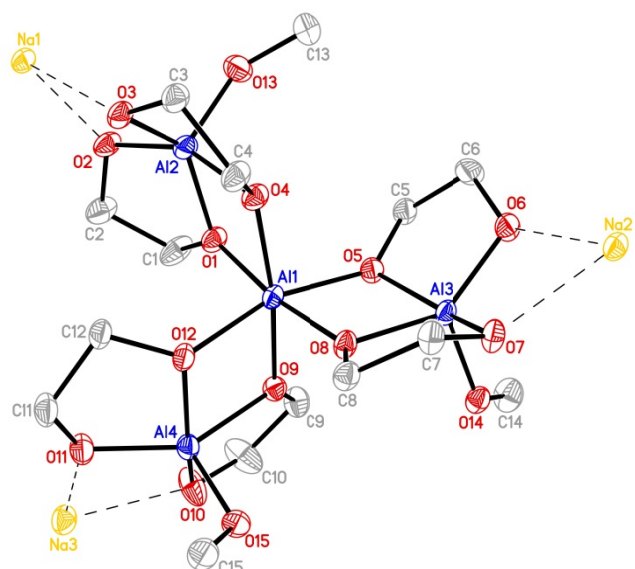


**Fig. 1** Asymmetric-unit structure of the aluminate complex  $\text{Na}_3[\text{Al}_4(\text{OCH}_3)_3(\text{OCH}_2\text{CH}_2\text{O})_6]$  comprising three  $^{[5]}\text{Al}$  moieties stitched together by a fourth  $^{[6]}\text{Al}$ . Hydrogen atoms are omitted for clarity, and thermal ellipsoids are set to 50% probability. Selected interatomic bond distances ( $\text{\AA}$ ) and bond angles ( $^\circ$ ): Al(2)-O(13): 1.7539(14), Al(3)-O(14): 1.7784(13), Al(4)-O(15): 1.7661(14), Al(4)-O(11): 1.7836(14), Al(4)-O(12): 1.9122(13), Al(1)-O(1): 1.8714(13), and Al(1)-O(8): 1.9014(13); Al(1)-O(12)-Al(4): 101.24(6), and Al(1)-O(9)-Al(4): 103.42(6).

The interatomic distances selectively shown in Fig. 1 caption signify a range of Al-O bond strengths for various ligands and Al species. Bonding behaviors in  $^{[5]}\text{Al}$  moieties are a contracted Al-O bond to the monodentate methanolate oxygens [Al-O, 1.7539(14)-1.7784(13)  $\text{\AA}$ ] compared with bidentate glycolate Al-O bonds [1.7836(14)-1.9122(13)  $\text{\AA}$ ]. The shorter Al-O bonds observed for the glycolates invariably involve O atoms with strong Coulombic  $\text{Na}^+\text{-O}$  interactions. In contrast, the Al-O bond length in the  $^{[6]}\text{Al}$  moiety ranges from 1.8714(13) [Al(1)-O(1)] to 1.9014(13)  $\text{\AA}$  [Al(1)-O(8)]. By comparison, an average Al-O bond length in zeolites is 1.74  $\text{\AA}$ , which is slightly shorter than the shortest Al-O distance in this aluminohydroxylate anion. Additionally, the average O-Al-O bond angle ( $109.5^\circ$  in close proximity to the tetrahedral value of  $109.4^\circ$ ) in zeolites<sup>15</sup> lies intermediate among all of the O-Al-O bond angles in this Al complex due to the severe structural distortion of the latter Al polyhedra. On the other hand, the Al-O-Al linkage is generally forbidden in aluminosilicate zeolitic frameworks according to the Loewenstein rule<sup>16</sup> obeying Pauling's electrostatic valence principle<sup>16</sup> with several exceptions for naturally occurring zeolite minerals (e.g., analcime,<sup>17</sup> stilbite<sup>18</sup> and lazurite<sup>19</sup>). Zeolites have a representative T-O-T [T (tetrahedral) = Al or Si] bond angle of  $141^\circ$ <sup>15</sup> which is much larger than Al(1)-O-Al counterparts varying in a much narrower range from 101.24(6) to 103.42(6) $^\circ$ . The magnitude of the Coulombic electrostatic repulsive interaction ( $^{[4]}\text{Al}^-\text{-O-}^{[4]}\text{Al}^-$  electrostatic repulsion between Al anions in zeolites vs.  $^{[5]}\text{Al}^{0.67-}\text{-O-}^{[6]}\text{Al}^-$  one in the latter) can interpret this big angular difference and what enables the exact existence of Al-O-Al linkages in the Al complex as opposed to synthetic zeolites.

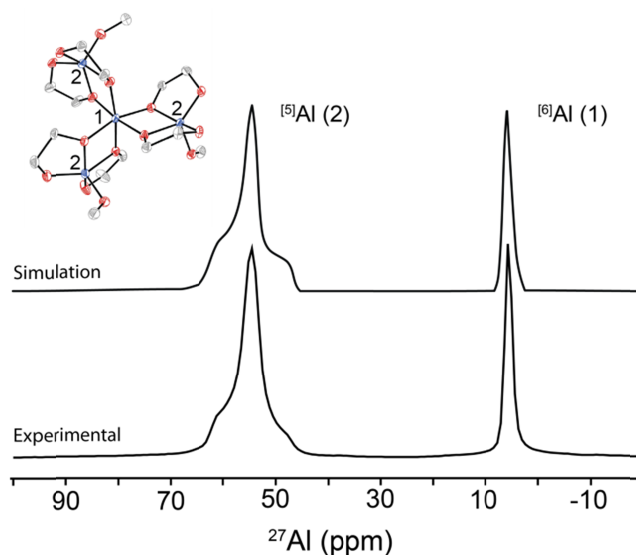


**Fig. 2**  $^{27}\text{Al}$  MAS NMR spectrum acquired at 16.4 T (experimental) and corresponding simulation of two distinct aluminium coordination environments, i.e., 5-coordinate ( $^{[5]}\text{Al}$ ) and 6-coordinate ( $^{[6]}\text{Al}$ ).

Corroborating the SCXRD studies, the  $^{27}\text{Al}$  MAS NMR spectrum (Fig. 2) reveals two highly crystalline Al sites with a 1:3 ratio. The simulated  $^{27}\text{Al}$  NMR parameters for Site 1 ( $\delta_{\text{iso}} = 6$  ppm and a quadrupolar coupling constant of  $C_Q < 2$  MHz) are consistent with the octahedral environment determined by SCXRD. The second site therefore corresponds to the  $^{[5]}\text{Al}$  nuclei exhibiting a unique  $\delta_{\text{iso}} = 62$  ppm, a moderate  $C_Q = 5.5$  MHz and an asymmetry parameter,  $\eta = 0.95$ . The larger quadrupolar coupling for Site 2 causes a second order broadening which spans 3 kHz at the base. The larger  $C_Q$  and  $\eta$  are due to the greater distortion/asymmetry of the  $^{[5]}\text{Al}$  sites relative to the  $^{[6]}\text{Al}$  one. The unusual chemical shift is observed for the  $^{[5]}\text{Al}$  environment as other well-characterized Al-containing oxides are generally located between 20 and 50 ppm.<sup>10</sup> The unique chemical shift is believed to arise from the very unique local structure of the asymmetric unit (Fig. 1) and large Coulombic interactive forces (*vide supra*) whereby one  $^{[6]}\text{Al}$  is surrounded by three  $^{[5]}\text{Al}$ s creating a localized pseudo-three-fold symmetry. Each  $^{[5]}\text{Al}$  species is further capped by two bidentate glycolate ligands causing the shift to a higher frequency. Such a substantial increase in chemical shift is not uncommon as these large shifts have also been observed in a 6-coordinate tris(tropolonato)aluminum(III)<sup>20</sup> and 4-coordinate high-alumina cements.<sup>21</sup>

As illustrated in Figs. 1 and S1b, the two glycolate chelators constitute the pyramidal base with a monobasic methanolate occupying the fifth position at the apex, forming the primary BU. The pseudo-pyramidal basal plane is defined *via* the oxygen atoms of the chelating glycolates with the central  $\text{Al}^{3+}$  ions 0.34-0.38  $\text{\AA}$  above this rectangular plane. Accordingly,  $^{13}\text{C}$  MAS NMR spectra identified two distinct regions representing the various bidentate glycolate carbons (14 crystallographic carbons) (62-68 ppm) and the methanolate carbons (5 crystallographic carbons) residing at the apex of the rectangular pyramidal  $^{[5]}\text{Al}$  polyhedral (Fig. 3). The  $^{13}\text{C}$  solid-state NMR spectra indicate a highly ordered crystalline structure with  $^{13}\text{C}$  line-widths approaching  $\sim 0.5$  ppm ( $\sim 65$  Hz). Precise assignment is difficult due to the 19 crystallographic carbons

being quite similar in chemical environment. We note however two of the three methanolate carbons were found in a disordered environment (Fig. S1a), hence we speculate these to be assigned to the higher frequency resonance ( $\sim 55$  ppm) while the lower frequency resonance ( $\sim 54$  ppm) is assigned to the ordered resonance as the area ratio is found close to 2:1. The glycolate carbons represent seven distinct glycolate ligands, five in an ordered arrangement and two in a position-disordered configuration. However, it is interesting that the glycolate region approximately resembles a 1:2:2:1:1 ratio with respect to one another. The absence of  $J$ -coupling (*n.a.*  $^{13}\text{C}$ , 1.1%) with the combination of MAS and high-power  $^1\text{H}$  decoupling ( $\gamma B_1$  ( $^1\text{H}$ ) = 100 kHz) removes the remaining chemical shielding and dipolar anisotropies, leaving behind pure isotropic chemical shift information. Without further symmetry constraints available, the exact assignment is not currently attainable.

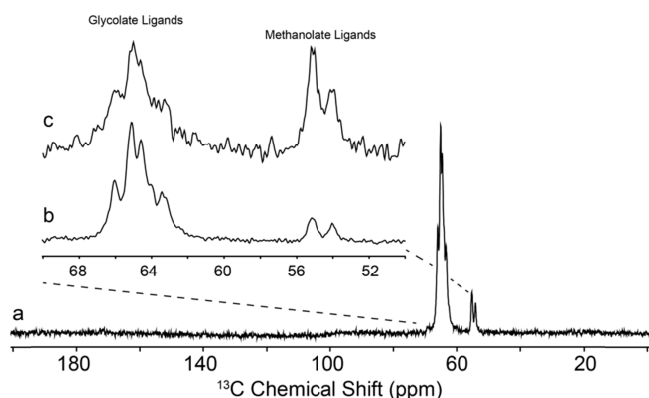


**Fig. 3**  $^{13}\text{C}$  MAS NMR spectrum of the Al complex acquired using  $^{13}\text{C}\{^1\text{H}\}$  cross-polarization (CP) at 11.7 T (a). Inset represents a magnified region (50–70 ppm) with the glycolate and methanolate ligands identified using CP (b) and direct (Bloch) detection (c) over 8 and 60 h, respectively.

The assembly process of the crystal structure of the aluminate complex from a 1D chain to a 2D plane and to a 3D architecture is sequentially illustrated in Fig. 4. Fig. 4a shows the 1D chain building block comprising 3 AUs that are held together by two coordinatively saturated 6-coordinate  $\text{Na}^+$  cations with respect to Oxygens, forming the in-plane Na-O ionic bonds. To completely establish the coordinatively saturated structure, a fraction of under-coordinated 2-coordinate  $\text{Na}^+$  species on each AU functions as cross-linker to bind the adjacent chains together by out-of-plane Na-O ionic interactions into one 2D layer parallel to (110) crystal plane (Fig. 4b). As shown in Figs. 4c and S2 both highlighting a layered structure, the 3D structure viewed along the crystallographic [110] axis is constructed by periodically stacking two (110) planes layer-by-layer with the interlayers cross-linked by the out-of-plane coordinatively unsaturated Na-O ionic bonds remaining on the (110) planes. Likewise, the ( $\bar{1}10$ )-parallel interlayers are also bound together by different out-of-plane  $\text{Na}^+$  cations (Fig. 4c).

The experimental PXRD pattern of this sample closely matches the simulated XRD pattern derived from the SCXRD structure, suggesting the high phase purity of our powdered sample (Fig. 5). The experimental PXRD pattern exhibits a predominantly intense (110) reflection at  $10.5^\circ$   $2\theta$  (8.42 Å in (110) interplanar  $d$ -spacing) without any noticeable background intensity, characteristic of a (110)-dominant and well-

crystallized Al complex. The typical (110) basal series peak until (220) manifests a material of a well-organized layered structure. As indicated in Figs. S2 and S3, the orientation of the chosen parallel layers is consistent with the PXRD-characterized result. It is worth noting here that we select (110) as the basal plane of these layers instead of ( $\bar{1}10$ ). Also, the interlayer spacing of this material could be finely tuned either by delamination or by substituting out-of-plane  $\text{Na}^+$  cations through post ion-exchange or direct synthetic means, thus making it a potential adsorbent.

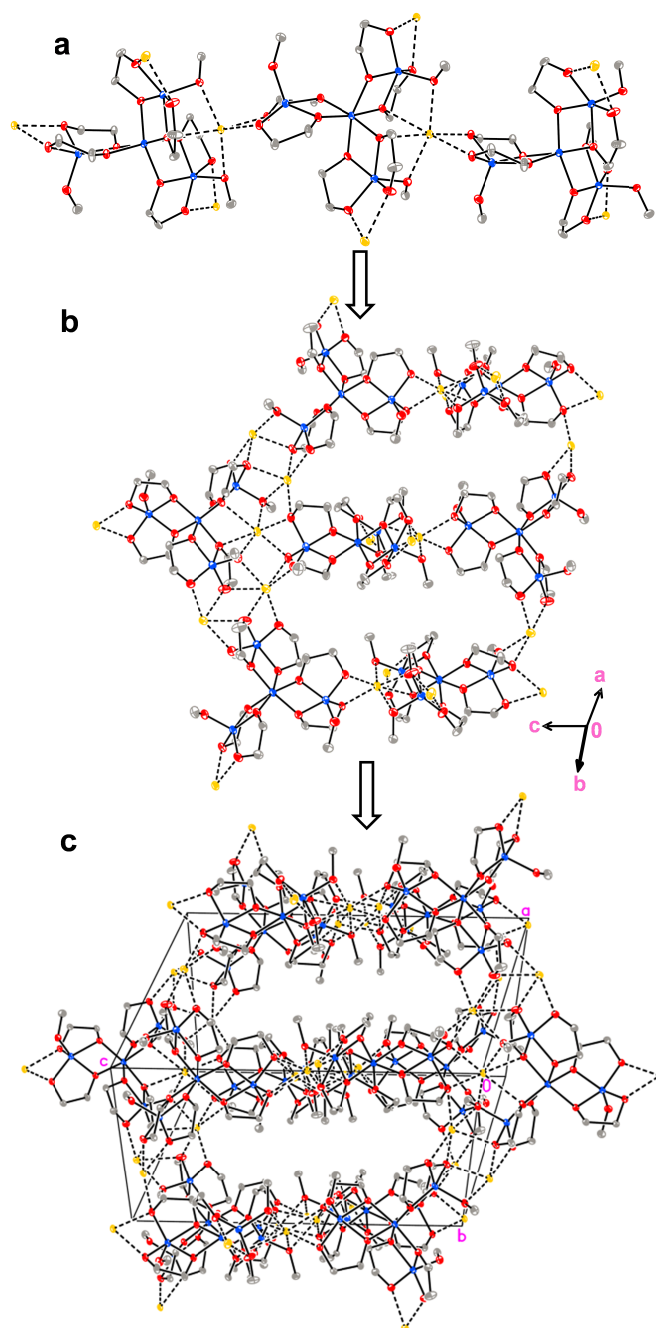


**Fig. 4** Flowchart of the assembly process of the crystal structure from a 1D chain along  $c$  axis (a), to a 2D viewed parallel to (110) plane (b), and to a 3D viewed along the [110]

axis highlighting the layered structure (c). Hydrogen atoms are omitted for clarity. Blue: Al; red: O; gray: C; and yellow: Na.

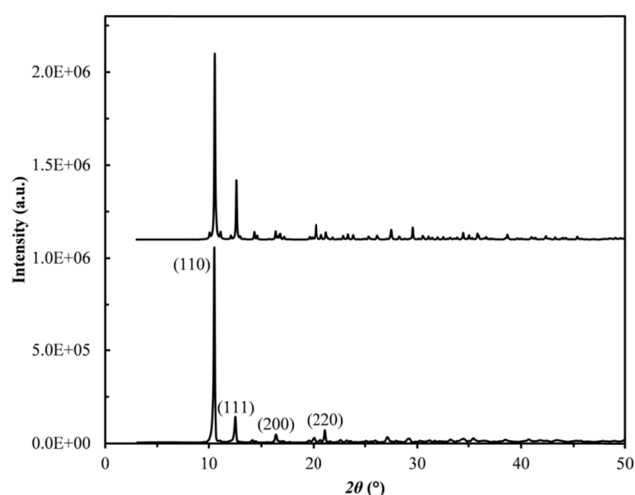


**Fig. 5** Top: Simulated PXR pattern of as-synthesized layered sodium aluminoolcoholate single crystal, and Bottom: Experimental PXR pattern of the same powders. Well-ordered and typical 110 basal series peaks from (110) to (220) in both patterns.

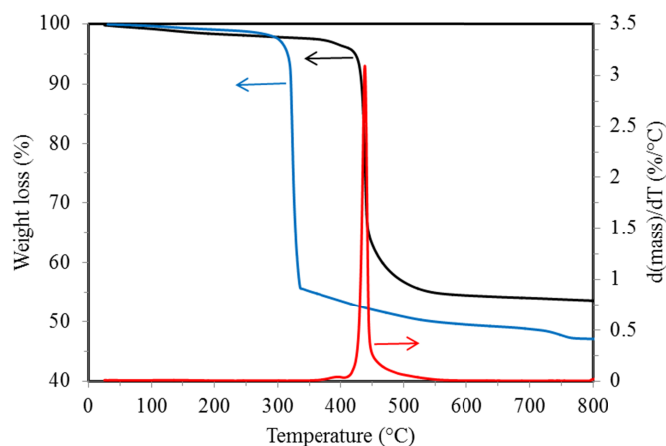


**Fig. 6** TGA profiles of the Al complex in flowing  $N_2$  (black curve) and air streams (blue curve). The red curve represents the DTG (derivative thermogravimetry) for the black trace.

The thermal stability of the Al complex was evaluated by TGA operating in both flowing  $N_2$  and air streams, as shown in Fig. 6. Under flowing  $N_2$  atmosphere, between 25 and 350 °C, there exhibited *ca.* 2.3% weight loss likely corresponding to the evaporation of physisorbed water, occluded MeOH solvent, and/or loosely bound methanolate-like ligands. With increasing temperature, two distinguishable weight losses were observed before the final plateau based on the DTG profile. The first very small weight loss centered at *ca.* 380 °C (~1.2%) is likely due to the loss of a small portion of relatively strongly bound methanolate-like ligands. A dramatic weight loss associated with the framework collapse was then observed between 405 and 550 °C with a temperature inflection point at 438 °C. In contrast, under flowing air, the onset degradation temperature occurred at 300 °C, and an overall weight loss of 52.9% was observed, ultimately leading to the whitened decomposition powders. The theoretical weight loss for the conversion from

$C_{15}H_{33}Al_4Na_3O_{15} \cdot 0.1CH_4O$  to a stoichiometric oxide  $3NaAlO_2 \cdot 0.5Al_2O_3$  is 53.1%, which agrees well with the total weight loss occurring in the air stream, but differs from that of 46.2% in the  $N_2$  stream. The reason for this discrepancy is the concomitant formation of minor carbon residues (~6.5%) in the anaerobic conditions, as indicated by the blackened appearance of the end powders. As such, this layered material is quite thermally stable under  $N_2$  or air atmosphere. On the other hand, part of the in-plane  $Na^+$  counterions and framework  $Al^{3+}$  ions are roughly sandwiched by alkoxides (Fig. 4c), thereby inhibiting to some extent the hydrolysis of  $Al^{3+}$  ions upon contact with moisture in favor of its hydrolytic stability accordingly.

Fig. 7 showed the ATR-FTIR spectrum of the Al complex. A very weak broad O-H band in the region of 3500-3200  $cm^{-1}$  is marginally visible, indicating very low content of free alcohol or non-fully-condensed hydroxyl residues present in the crystals, and consequently very weak hydrogen bonding interaction arises. This result is in good agreement with the SCXRD and TGA analyses. The strong band at 2950-2850  $cm^{-1}$  is due to the alkyl C-H stretching vibrations. By analogy with zeolites, the vibrational frequencies of the zeolite lattice, which result from the stretching and bending modes of the T-O units, are observed in the range between 200 and 1500  $cm^{-1}$ .<sup>22</sup> Since the average Al-O bond length in zeolites is shorter than those in the current Al complex (*vide supra*), the Al-O vibrational frequencies in the former shift to slightly higher wavenumbers than the latter. Hence, we attribute the absorption band at 500-1460  $cm^{-1}$  to the Al-O vibrational frequencies of the Al complex. Obviously, no free hydroxyl groups present in its empirical formula other than those from the occluded MeOH solvent (*ca.* 10% occupancy, *cf.* Fig. S1a) account for the fewer hydrogen bonding interactions in the crystal lattice, as confirmed by ATR-FTIR. Therefore, it justifies the effectiveness of the sodium methoxide catalyst in full condensation.

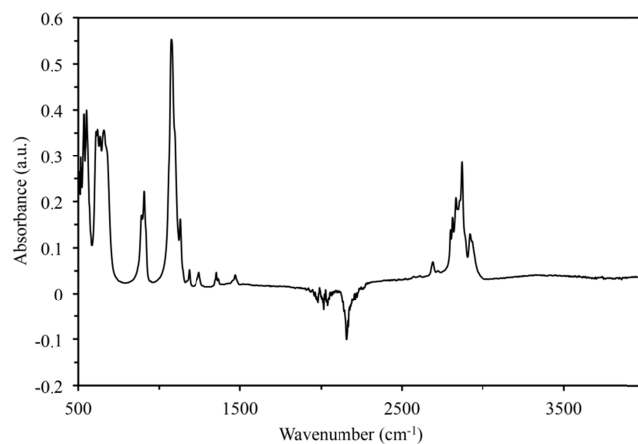


**Fig. 7** ATR-FTIR spectrum of the Al complex recorded under ambient condition.

In addition, the preliminary findings suggest that this Al complex is a useful precursor towards the facile preparation of high-surface-area alumina powders by a fast pyrolysis technique (10 °C/min), giving hierarchically porous alumina grains. Figs. 8 and 9 show the  $N_2$  sorption isotherms, and PSD and cumulative pore volume of the pyrolyzed Al complex precursor without any aqueous leaching, respectively. It is found that the  $S_{BET}$  is up to 91.7  $m^2/g$  together with the  $V_t$  of 0.103 ml/g for pores smaller than 41.8 nm (width) at an RP of

0.95. After experiencing aqueous leaching of  $\text{NaAlO}_2$  component, the  $S_{\text{BET}}$  of the resulting alumina powders is slightly enhanced to  $104.9 \text{ m}^2/\text{g}$  with the corresponding  $V_t$  nearly unchanged (not shown here). Moreover, the  $V_{\text{meso}}$  of the unwashed sample dominates the total pore volume accounting for 86.4%. As shown in Fig. 9, the mesopore radius at the maximal PSD is  $19.15 \text{ \AA}$ .

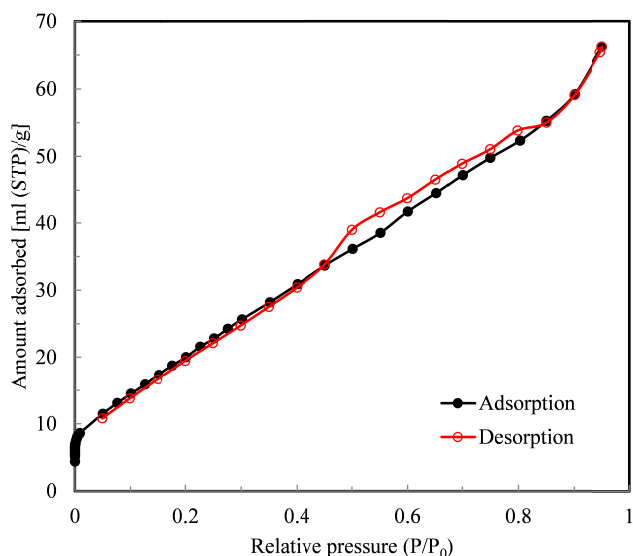


**Fig. 8**  $\text{N}_2$  adsorption/desorption isotherms of the pyrolyzed Al complex without any aqueous rinse post treatment.

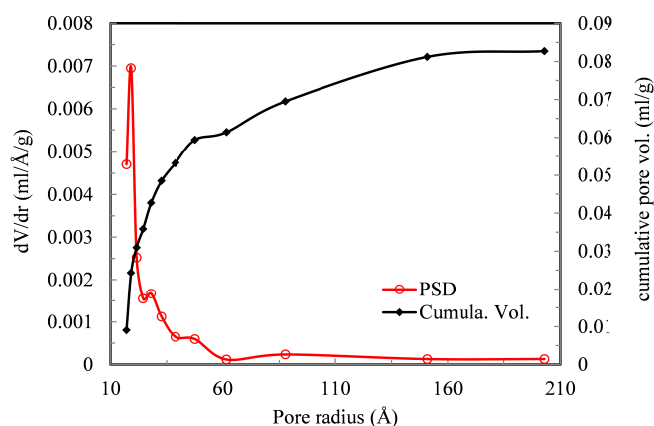


**Fig. 9** PSD and cumulative pore volume of the pyrolyzed Al complex without any aqueous rinse post treatment.

## Conclusions

In summary, a new well-crystallized and phase-pure tetranuclear Al complex was successfully synthesized by utilizing a modified transesterification reaction. Its layered crystal architecture comprising a network of the combination of  $^{51}\text{Al}$  and  $^{61}\text{Al}$  geometries was determined via SCXRD analysis and further corroborated via  $^{27}\text{Al}$  and  $^{13}\text{C}$  MAS NMR spectroscopies. Another feature lies in that the Al-O-Al linkage is allowed in its crystal structure as a result of slightly weakened electrostatic repulsive interactions between Al centers as compared with synthetic zeolites. The coordinatively

unsaturated Al binding sites within the porous lattice and high thermal stability could be an attractive property for the potential applications of this material as an adsorbent. In addition, the versatile synthetic methodology proposed in this study is expected to open up a new avenue to elegantly design new porous metal-organic materials. Finally, this study provides a new route for the efficient fabrication of highly nanoporous alumina powders with hierarchical micro-/meso-porosity.

## Experimental Section

### 1. Solvothermal synthesis

A transesterification synthetic strategy was formulated to prepare this layered Al complex  $\text{Na}_3[\text{Al}_4(\text{OCH}_3)_3(\text{OCH}_2\text{CH}_2\text{O})_6]$ . No special care was taken to exclude the exposure to extraneous moisture, and all manipulations were carried out in a well-ventilated fume hood. All chemicals were purchased from Sigma-Aldrich and used as received.

A recipe of  $\text{Al}(\text{OC}_2\text{H}_5)_3 : 3\text{EG} : \text{NaOCH}_3 : 15\text{CH}_3\text{OH}$  on a molar basis was originally developed. In the synthesis, 2.93 g of sodium methoxide powders (97%) were completely dissolved in 23.57 g of anhydrous methanol solvent (99.8%) under stirring before the addition of 8.79 g of aluminium ethoxide powders (97%). When the dissolution of the Al source was complete, 9.90 g of EG was rapidly added dropwise under intense agitation. The aging was maintained overnight at room temperature (RT) under stirring in a tightly sealed autoclave to ensure adequate homogenization. The solvothermal synthesis was then statically carried out at  $181^\circ\text{C}$  under autogenous pressure for 5 d. The solid fraction was recovered *via* vacuum suction filtration and successively rinsed with anhydrous methanol, anhydrous tetrahydrofuran (THF, 99.9%), and further anhydrous methanol. The collected solid was vacuum dried at  $80^\circ\text{C}$  for 10 h yielding 3.5 g of dry powders which were stored in a desiccator for future structural characterization. The colourless crystalline product appeared as polycrystalline powders with a few sparse X-ray-quality single crystals (e.g.,  $0.11 \times 0.04 \times 0.01 \text{ mm}^3$  in dimension). It is worth noting that the above synthetic protocol was not optimized as the approach proposed here is robust and readily reproducible.

### 2. Pyrolytic preparation of porous alumina powders

To achieve porous alumina composite for  $\text{N}_2$  sorption measurement, fast pyrolysis was conducted on the Al complex precursor (several tens of mg) in a flowing air atmosphere ( $\sim 25 \text{ ml/min}$ ) in a TGA furnace using a ramping rate of  $10^\circ\text{C/min}$  up to  $900^\circ\text{C}$  and a soaking duration of 3 min. Part of the pyrolyzed white powders were subsequently subjected to adequate aqueous rinse overnight at room temperature under stirring to yield pure alumina product.

### 3. Single-crystal X-ray diffraction (SCXRD)

Low-temperature ( $-173^\circ\text{C}$ ) XRD data comprising  $\varphi$ - and  $\omega$ -scans were collected using a Bruker-AXS X8 Kappa Duo diffractometer coupled with a Smart Apex II CCD detector with an  $I\mu\text{S}$  source of  $\text{Mo } K_\alpha$  radiation ( $\lambda = 0.71073 \text{ \AA}$ ). The structure was solved by direct methods using SHELXS<sup>23</sup> and refined against  $F^2$  on all data by full-matrix least squares with SHELXL-97<sup>24</sup> using established refinement strategies.<sup>25</sup> All non-hydrogen atoms were refined anisotropically. The positions of all hydrogen atoms were calculated geometrically and refined using a riding model. The isotropic displacement parameters of all hydrogen atoms were fixed to be 1.2 times the  $U_{\text{eq}}$  value of the atom to which they are bound (1.5 for methyl groups). The representations of the positional disorders of some atoms and the asymmetric unit of the title crystal showing the empirical formula  $\text{C}_{15}\text{H}_{33}\text{Al}_4\text{Na}_3\text{O}_{15} \cdot 0.1\text{CH}_4\text{O}$  involving  $\sim 10\%$  occupancy of MeOH solvent molecule were illustrated in Fig. S1a.

#### 4. Solid-state NMR (ssNMR)

Solid-state NMR experiments were performed at either 11.7 (500 MHz,  $^1\text{H}$ ) or 16.4 T (697 MHz,  $^1\text{H}$ ) using a home-built NMR spectrometer (courtesy of Dr. D. Ruben, FBML-MIT) and a 3.2 mm Chemagnetics triple-resonance MAS probe for  $^{13}\text{C}$  and  $^{27}\text{Al}$ , respectively. The crystalline sample was ground using an agate mortar and pestle under dry atmosphere and packed quickly into a 3.2 mm (o.d.)  $\text{ZrO}_2$  rotor (~26  $\mu\text{l}$  sample).  $^{27}\text{Al}$  spectra were acquired at a spinning frequency,  $\omega_r = 16000(4)$  Hz and between 4096 and 65536 co-added transients. Recycle delays were optimized using a saturation recovery experiment and set to 1.2 s using a Bloch<sup>26</sup> experiment with a short quantitative tip angle ( $14^\circ$ ) and 3.0 s using a Hahn echo<sup>27</sup> sequence ( $^{27}\text{Al}$   $\gamma B_1 = 60$  kHz). Non-spinning experiments (not shown here) were also collected using identical parameters above (Hahn-echo) with 83 kHz of  $^1\text{H}$  continuous-wave decoupling.  $^{27}\text{Al}$  spectra were referenced relative to 1.1 M  $\text{Al}(\text{NO}_3)_3$  solution at 0 ppm.<sup>28</sup>  $^{13}\text{C}\{^1\text{H}\}$  CP<sup>29</sup> and direct detection spectra were acquired at  $\omega_r = 13450(1)$  Hz, 8192 co-added transients and recycle delay of 3 and 25 s, respectively. The contact time during the CP experiment was set to 1.5 ms. Both experiments were acquired using high-power ( $^1\text{H}$   $\gamma B_1 = 100$  kHz) two-pulse phase modulation (TPPM)<sup>30</sup>  $^1\text{H}$  decoupling during acquisition.  $^{13}\text{C}$  spectra were referenced using solid adamantane to 40.49 ppm.<sup>31</sup> The magic angle within the probe was set using the  $^{79}\text{Br}$  resonance of solid KBr and shimmed using adamantane prior to signal acquisition. The sample temperature was regulated between 22 and 26  $^\circ\text{C}$  during acquisition. All spectra were processed using RNMTP data processing software; quadrupolar line shapes were simulated using either WSOLIDS or SPINEVOLUTION software packages.<sup>32</sup>

#### 5. Powder X-ray diffraction (PXRD)

PXRD pattern was taken using a PANalytical X'Pert Pro Multipurpose Diffractometer in reflectance Bragg-Brentano geometry at 45 kV and 40 mA using Ni-filtered  $\text{Cu } K\alpha$  radiation ( $\lambda = 1.54$  Å). The data collection was carried out at a constant temperature of 25  $^\circ\text{C}$  with a step increment of  $0.084^\circ 2\theta$ , a counting time of 6.4 s/step, and the  $2\theta$  angular range from 3 to  $50^\circ$ .

#### 6. Thermogravimetric analysis (TGA)

The sample with an initial mass of 18.48 mg was heated in a Pt pyrolytic pan at a constant ramping rate of 10  $^\circ\text{C}/\text{min}$  from ambient temperature up to 800  $^\circ\text{C}$  on a Discovery TG analyzer (TA Instruments) in flowing  $\text{N}_2$  and air atmospheres both set to 25 ml/min. The isothermal duration at 800  $^\circ\text{C}$  was set to 3 min.

#### 7. Attenuated total reflectance-Fourier transform infrared spectroscopy (ATR-FTIR)

IR absorbance spectrum was collected on the Al complex using a Nexus 870 FT-IR E.S.P. spectrometer (Thermo Scientific) equipped with an ATR accessory with a single reflection diamond crystal. The FT-IR chamber was flushed constantly with flowing  $\text{N}_2$  stream (ca. 0.71  $\text{m}^3/\text{h}$ ). Scans at a spectral resolution of  $\pm 4$   $\text{cm}^{-1}$  were taken at RT on a self-supporting sample disc from 4000 to 500  $\text{cm}^{-1}$ . Sixteen scans were averaged, and the resulting spectrum was background subtracted.

#### 8. Gas sorption analysis on the pyrolyzed Al complexes with and without aqueous rinse

Gas sorption studies were carried out to investigate the textural properties of the pyrolyzed products ( $3\text{NaAlO}_2 \cdot 0.5\text{Al}_2\text{O}_3$ ) with and without aqueous rinse. The  $\text{N}_2$  sorption measurement was performed at -196  $^\circ\text{C}$  using an Autosorb iQ2 automated gas sorption analyzer (Quantachrome). Before adsorption run, the

sample was degassed under vacuum (ca. 0.2 Pa) at 370  $^\circ\text{C}$  for 12 h. Afterwards, a proper glass rod filler was inserted in a sample cell to minimize the cell dead voids. The BET (Brunauer, Emmett, and Teller) surface area ( $S_{\text{BET}}$ ) was obtained by applying the BET equation to a relative pressure (RP) range of 0.05-0.30 on the adsorption branch. The total pore volume ( $V_t$ ) was evaluated from the adsorbed  $\text{N}_2$  amount at a maximum RP of 0.95. The pore size distribution (PSD) was calculated by the BJH (Barrett, Joyner, and Halenda) method on the desorption branch. The micropore volume ( $V_{\text{micro}}$ ) was determined by applying the D-R (Dubinin-Radushkevich) equation to an RP range of 0.00005-0.009 on the adsorption isotherm.

#### Acknowledgements

This research was supported by the U.S. Department of Energy's Advanced Research Projects Agency-Energy (ARPA-E) under control No. 0471-1627. NMR studies were supported by the National Institute of Health through Grants EB-001960 and EB-002026 (R.G.G.). The diffractometer was purchased with the funding from the National Science Foundation under Grant No. CHE-0946721. V.K.M. is grateful to the Natural Sciences and Engineering Research Council of Canada for a Postdoctoral Fellowship.

#### Notes

<sup>1</sup> Department of Mechanical Engineering, Massachusetts Institute of Technology, Cambridge, Massachusetts 02139, USA. E-mail: xsli@mit.edu; enwang@mit.edu. Tel: +1-617-324-3311.

<sup>2</sup> Department of Chemistry, Massachusetts Institute of Technology.

<sup>3</sup> Francis Bitter Magnet Laboratory, Massachusetts Institute of Technology.

† Electronic Supplementary Information (ESI) available: Representations of the methanol occupancy and positional disorders of some atoms. Packing structures along  $c$  and  $[\bar{1}10]$  axes. CIF file for the aluminate complex. CCDC 955650. For ESI and crystallographic data in CIF or other electronic format. See DOI: 10.1039/b000000x/

#### References

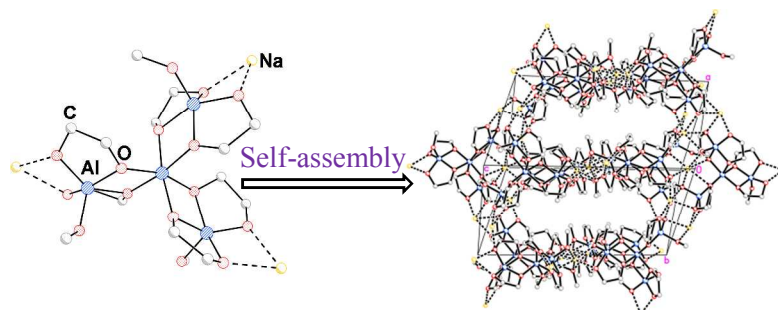
- G. G. Amatucci, J. M. Tarascon and L. C. Klein, *J. Electrochem. Soc.*, 1996, **143**, 1114-1123.
- Z. Xu, J. Fan, S. Zheng, F. Ma and D. Yin, *J. Environ. Qual.*, 2009, **38**, 1302-1310.
- N. Barrabes, D. Cornado, K. Föttinger, A. Dafinov, J. Llorca, F. Medina and G. Rupprechter, *J. Catal.*, 2009, **263**, 239-246.
- B. Ballarin, M. Berrettoni, I. Carpani, E. Scavetta and D. Tonelli, *Anal. Chim. Acta*, 2005, **538**, 219-224.
- R. Ma, Y. Bando and T. Sasaki, *J. Phys. Chem. B*, 2004, **108**, 2115-2119.
- Y. Hudiono, S. Choi, S. Shu, W. J. Koros, M. Tsapatsis and S. Nair, *Micropor. Mesopor. Mater.*, 2009, **118**, 427-434.
- D. M. Bibby and M. P. Dale, *Nature*, 1985, **317**, 157-158.
- (a) R. M. Laine, K. Y. Blohowiak, T. R. Robinson, M. L. Hoppe, P. Nardi, K. Kampf and J. Uhm, *Nature*, 1991, **353**, 642-644; (b) S. D. Kinrade, J. W. D. Nin, A. S. Schach, T. A. Sloan, K. L. Wilson and C. T. G. Knight, *Science*, 1999, **285**, 1542-1545; (c) B. Herreros, S. W. Carr and J. Klinowski, *Science*, 1994, **263**, 1585-1587; (d) K. Y. Blohowiak, D. R. Treadwell, B. L. Mueller, M. L. Hoppe, S. Jouppi, P.

- Kansal, K. W. Chew, C. L. S. Scotto, F. Babonneau, J. Kampf and R. M. Laine, *Chem. Mater.*, 1994, **6**, 2177-2192; (e) A. R. Bassindale, M. Sohail, P. G. Taylor, A. A. Korlyukov and D. E. Arkhipov, *Chem. Commun.*, 2010, **46**, 3274-3276; (f) C. Kobelt, C. Burschka, R. Bertermann, C. F. Guerra, F. M. Bickelhaupt and R. Tacke, *Dalton Trans.*, 2012, **41**, 2148-2162.
- 9 (a) M. C. Cruickshank and L. S. D. Glasser, *J. Chem. Soc., Chem. Commun.*, 1985, **2**, 84-85; (b) M. C. Cruickshank and L. S. D. Glasser, *Acta Crystallogr. Sect. C: Cryst. Struct. Commun.*, 1985, **C41**, 1014-1017; (c) L. B. Alemany and G. W. Kirker, *J. Am. Chem. Soc.*, 1986, **108**, 6158-6162; (d) G. J. Gainsford, T. Kemmitt and N. B. Milestone, *Inorg. Chem.*, 1995, **34**, 5244-5251.
- 10 K. J. D. Mackenzie and M. E. Smith, in *Multinuclear Solid-State NMR of Inorganic Materials*, ed. R. W. Cahn, Pergamon, Oxford, 2002, vol. 6, pp. 271-324.
- 11 (a) J. A. Francis, S. G. Bott and A. R. Barron, *J. Organometal. Chem.*, 2000, **597**, 29-37; (b) J. Pauls and B. Neumüller, *Z. Anorg. Allg. Chem.*, 2000, **626**, 270-279; (c) H. Nöth, A. Schlegel and Max Suter, *J. Organometal. Chem.*, 2001, **621**, 231-241; (d) T.-C. Liao, Y.-L. Huang, B.-H. Huang and C.-C. Lin, *Macromol. Chem. Phys.* 2003, **204**, 885-892; (e) W. Ziemkowska, S. Kucharski, A. Kolodziej and R. Anulewicz-Ostrowska, *J. Organometal. Chem.*, 2004, **689**, 2930-2939; (f) J. Pauls, E. Irvani, P. Köhl and B. Neumüller, *Z. Anorg. Allg. Chem.*, 2004, **630**, 876-884; (g) Z. Janas, L. B. Jerzykiewicz, P. Sobota, K. Szczegot and D. Wicniewska, *Organometal.*, 2005, **24**, 3987-3994; (h) L. Dostál, R. Jambor, I. Císařová, J. Merna and J. Holeček, *Appl. Organometal. Chem.*, 2007, **21**, 688-693.
- 12 M. J. Hampden-Smith, D. S. Williams and A. L. Rheingold, *Inorg. Chem.*, 1990, **29**, 4076-4081.
- 13 J. Romanski, P. Nowak, K. Kosinski and J. Jurczak, *Tetrahedron Letters*, 2012, **53**, 5287-5289.
- 14 M. L. Hoppe, R. M. Laine, J. Kampf, M. S. Gordon and L. W. Burggraf, *Angew. Chem. Int. Ed.*, 1993, **32**, 287-289.
- 15 R. W. Joyner, A. D. Smith, M. Stockenhuber and M. W. E. Van Den Berg, *Stud. Surf. Sci. Catal.*, 2004, **154**, 1406-1410.
- 16 W. Loewenstein, *Am. Mineral.*, 1954, **39**, 92-96.
- 17 X. Cheng, P. Zhao and J. F. Stebbins, *Am. Mineral.*, 2000, **85**, 1030-1037.
- 18 J. F. Stebbins, P. Zhao, S. K. Lee and X. Cheng, *Am. Mineral.*, 1999, **84**, 1680-1684.
- 19 J. Klinowski, S. W. Carr, S. E. Tarling and P. Barnes, *Nature*, 1987, **330**, 56-58.
- 20 R. W. Schurko, R. E. Wasylshen and H. Foerster, *J. Phys. Chem. A*, 1998, **102**, 9750-9760.
- 21 J. Skibsted, E. Henderson and H. J. Jakobsen, *Inorg. Chem.*, 1993, **32**, 1013-1027.
- 22 A. Jentys and J. A. Lercher, *Stud. Surf. Sci. Catal.*, 2001, **137**, 345-386.
- 23 G. M. Sheldrick, *Acta Crystallogr.*, 1990, **A46**, 467-473.
- 24 G. M. Sheldrick, *Acta Crystallogr.*, 2008, **A64**, 112-122.
- 25 P. Müller, *Crystallogr. Rev.*, 2009, **15**, 57-83.
- 26 F. Bloch, *Phys. Rev.*, 1946, **70**, 460-474.
- 27 E. L. Hahn, *Phys. Rev.*, 1950, **80**, 580-594.
- 28 R. K. Harris and E. D. Becker, *J. Magn. Reson.*, 2002, **156**, 323-326.
- 29 A. Pines, J. S. Waugh and M. G. Gibby, *J. Chem. Phys.*, 1972, **56**, 1776-1777.
- 30 A. E. Bennett, C. M. Rienstra, M. Auger, K. V. Lakshmi and R. G. Griffin, *J. Chem. Phys.*, 1995, **103**, 6951-6958.
- 31 C. R. Morcombe and K. W. Zilm, *J. Magn. Reson.*, 2003, **162**, 479-486.
- 32 (a) K. Eichele, *WSolids1-Solid State NMR Simulations*, Version 1.20.21, *Universität Tübingen*, 2013. (b) M. Veshtort and R. G. Griffin, *J. Magn. Reson.*, 2006, **178**, 248-282.

**One-pot Solvothermal Synthesis of Well-ordered Layered Sodium Aluminoalcoholate Complex: A Useful Precursor for the Preparation of Porous Al<sub>2</sub>O<sub>3</sub> Particles†**

Xiansen Li,<sup>\*1</sup> Vladimir K. Michaelis,<sup>2,3</sup> Ta-Chung Ong,<sup>2,3</sup> Stacey J. Smith,<sup>2</sup> Ian McKay,<sup>1</sup> Peter Müller,<sup>2</sup> Robert G. Griffin<sup>2,3</sup> and Evelyn N. Wang<sup>\*1</sup>

**Table of Contents (TOC) Entry**



A layered aluminate complex with combined 5-/6-coordinate Al centers is solvothermally synthesized *via* a modified transesterification mechanism, which is a valuable precursor toward the facile synthesis of high-surface-area alumina powders.